

# Wavelet Transform Modulus Maxima Based Fractal Correlation Analysis

D.C. Lin<sup>1</sup>, A. Sharif

<sup>1</sup>Department of Mechanical and Industrial Eng., Ryerson University,  
Toronto, ON, Canada

October 27, 2018

## Abstract

The wavelet transform modulus maxima (WTMM) used in the singularity analysis of one fractal function is extended to study the fractal correlation of two multifractal functions. The technique is developed in the framework of joint partition function analysis (JPFA) proposed by Meneveau et al. [1] and is shown to be equally effective. In addition, we show that another leading approach developed for the same purpose, namely, relative multifractal analysis, can be considered as a special case of JPFA at a particular parameter setting.

## 1 Introduction

Fluctuations in many natural and artificial phenomena are found to exhibit fractal characteristics. In applications, this has been characterized by the so-called singularity spectrum of some numerical or experimental data. To understand the dynamics underlying the fractal, it is not uncommon that multiple data capturing different aspects of the phenomenon of interest are used in the analysis. For example, velocity and temperature fluctuations are used to analyze the momentum and energy aspects of the multifractal hydrodynamic turbulence [1], blood pressure and heart rate fluctuations to analyze the cardiovascular aspect of the  $1/f$ -like power spectrum of the heart rate variability in humans [2], packet size and arrival time to analyze the congestion and connectivity aspects of the multifractal network traffic [3], and so on. For fractal analysis on natural objects, multiple data cross examination may provide the chance to examine the potential link of fractal fluctuation in the data. In

particular, one would suspect some degree of *fractal correlation* in the data if the fractal generating mechanisms associated with the data source are coupled together.

Essential to the notion of fractal correlation is the distinguishability of singularity spectra. There are fundamental and practical issues related to this subject. For example, consider a standard  $N_p$ -adic multinomial process on an interval. It is a multiplicative cascade constructed by repeatedly dividing the interval into equal  $N_p$  segments and assigning (probability) weights  $p_i, i = 1, \dots, N_p$ , from one generation to the next. Continuing this procedure *ad infinitum* leads to a limiting process with no density (almost surely) and intermittent spiking pattern. Its singularity spectrum  $f_\pi(\alpha)$  may be estimated by the Legendre transform of  $\tau_\pi(q) = -\log(\sum p_i^q) / \log(N_p)$ :

$$f_\pi(\alpha) = q\alpha - \tau_\pi(q)$$

where  $\alpha(q) = d\tau_\pi/dq$ . Now, consider a different  $N_m$ -adic cascade ( $N_m \neq N_p$ ) generated by weights  $m_i, i = 1, \dots, N_m$ , and its singularity spectrum  $f_\mu(\alpha)$ . If  $f_\pi(\alpha) = f_\mu(\alpha)$ , one must have

$$\sum p_i^q = \left( \sum m_i^q \right)^{\log(N_p) / \log(N_m)}.$$

However, no  $\{p_i\}$  and  $\{m_i\}$  can be found to satisfy this equation for all  $q$ . Thus, singularity spectra can in theory be distinguished, at least for the important class of multinomial processes. For more in-depth treatments and examples, see the excellent book by Pesin [4].

In practice, a different issue can arise. That is, two singularity spectra may be close to each other within the limit of finite precision. Consider again the cascades from above. Let  $\tau_\pi(-\infty) = \tau_\mu(-\infty)$ ,  $\tau_\pi(+\infty) = \tau_\mu(+\infty)$  (so  $\max(\{p_i\}) = \max(\{m_i\})^{\log(N_p) / \log(N_m)}$ ,  $\min(\{p_i\}) = \min(\{m_i\})^{\log(N_p) / \log(N_m)}$ ). Then,  $f_\pi(\alpha), f_\mu(\alpha)$  will agree at four important  $q$  values:  $-\infty, +\infty, 0, 1$ . With the rest of  $p_i$  and  $m_i$  chosen properly, they can be made almost indistinguishable (Fig. 1). This problem was addressed by Lévy-Léhel and Vojak who developed a much sharper mutual multifractal analysis to relate the singularity spectra to the generation of multinomial processes [5]. Riedi and Scheuring arrived at the similar relative multifractal analyses with further details on the numerical implementation [6]; see also [7, 8]. For experimental data, Meneveau et al. introduced a joint partition function analysis (JPFA) based on the 1D version introduced by Hentschel and Procaccia [9] and Halsey et al. [10]. With essentially the same procedure of estimating the singularity spectrum, these authors characterized fractal correlation in the small scale kinetic energy transfer, heat concentration and vorticity of the turbulent flow [1]. They implied that multiple cascades of more than

one variables are responsible for the fractal fluctuation in fluid turbulence; see also [11]. The JPFA has also been applied in diversified areas such as precision agriculture [12], soil property [13], and re-emerged in the general discussion of discrete scale invariance of the multinomial process [14].

In these past studies, JPFA as well as most singularity analyses were conducted on the assumption of one-dimensional multifractal measures and solved using the classical box counting procedure. Such applications can be limited in scope when, typically in the experimental study, the data is a fractal function that is not additive. For functions created by the integral of multinomial measure under  $C^\infty$  perturbation [15], Bacry et al. proved that the singularity analysis developed for fractal measures is equally applicable by using the so-called wavelet transform modulus maxima (WTMM) method. Later, the validity of WTMM was examined by Jaffard for any function [16]. Regarding WTMM, it was proved that (i) it can yield the upper bound estimate of the singularity spectrum for any function and (ii) it is exact for the so-called self-similar fractal function, as long as the so-called maxima lines are not too close to each others.

The purpose of this study is to introduce a joint WTMM method to carry out the JPFA of fractal correlation. The WTMM-based approach can provide an accessible and stable tool for estimating fractal fluctuation in multiple experimental data. We also point out that JPFA is a more general formulation. In particular, the existing relative multifractal analysis developed for the similar purpose relates to JPFA at a particular parameter setting. While the term correlation is normally linked to the second order statistics, fractal correlation as estimated from the singularity spectra is a property of moment of all orders. Indeed, the primary object of the analysis is the Hausdorff dimension  $f(\alpha_1, \alpha_2)$  of the support of observing Hölder exponents  $\alpha_1$  and  $\alpha_2$ . It will be shown that the set  $f(\alpha_1, \alpha_2)$  describes a two-dimensional surface whose level sets characterize the coupling of fractal generating mechanisms as well as the relative multifractal spectrum studied in the past.

Our results are organized into four sections. In the next section, the background of WTMM is first summarized. The extension to the WTMM-based JPFA and its connection to the relative multifractal spectrum are then given. The test of the method using multinomial cascades are presented in section 3. Concluding remarks are given in section 4.

## 2 WTMM–Based Fractal Correlation Analysis

### 2.1 WTMM Singularity Analysis

Singularity analysis is built on the notion of Hölder continuity of functions. Recall that a function  $x(t)$  is Hölder continuous of exponent  $\alpha'$  if there are  $\alpha', \delta_0, C \in \mathbf{R}^+$ , such that, for  $\delta < \delta_0$ ,

$$|x(t_0 + \delta) - x(t_0)| \leq C|\delta|^{\alpha'}.$$

In the neighborhood of  $x(t_0)$ , there exists a supremum  $\alpha(t_0)$  that (1) is valid for all  $\alpha' \leq \alpha(t_0)$ . The exponent  $\alpha(t_0)$  is the Hölder exponent of  $x(t)$  at  $t_0$ . Formally [15, 16], one can find an  $n$ th order polynomial  $P_n(t)$  and  $\alpha(t_0) \in [n, n + 1)$  such that

$$|x(t_0 + \delta) - P_n(t_0)| \leq C|\delta|^{\alpha(t_0)}. \quad (1)$$

It is evident that the Hölder exponent characterizes the differentiability of the function and, thus, how the function can fluctuate. For example,  $\alpha = +\infty$  for  $C^\infty$  functions,  $\alpha \in (n, n + 1)$  for functions that are only  $n$  times differentiable and  $\alpha < 1$  for functions that are non-differentiable. The  $\alpha < 1$  case draws the most attention since it means the function can fluctuate in large amplitude over short time intervals and gives rise to the so-called intermittent pattern witnessed in many physical systems. In this case, the Hölder exponent  $\alpha(t)$  is also known as the singularity exponent.

The natural tool to analyze the singularity property is by the wavelet transform:

$$T_\psi[x](t, a) = \frac{1}{a} \int_{-\infty}^{\infty} \psi\left(\frac{t' - t}{a}\right) x(t') dt' \quad (2)$$

where  $T_\psi[x](t, a)$  is the wavelet coefficient and  $\psi(t)$  is the analyzing wavelet. Muzy et al. showed that the exponent  $\alpha(t)$  can be estimated effectively using the supremum of  $|T_\psi[x]|$  along the so-called maxima line formed by the local wavelet modulus maxima [18]. Denote the set of maxima lines at scale  $a$  by  $\mathcal{L}(a) = \{l_1, l_2, \dots, l_{N(a)}\}$ . Bacry et al. proved that [15]

$$Z(a; q) = \sum_{l_i \in \mathcal{L}(a)} C_i^q \sim a^{\tau(q)} \quad (3)$$

where  $C_i = \sup_{(t,a) \in l_i} |T_\psi[x](t, a)|$  is the supremum of the modulus maxima along the maxima line  $l_i$ . For functions created by the integral of multinomial measures under  $C^\infty$  perturbations, it was shown that the Legendre transform of  $\tau(q)$  yields the Hausdorff dimension of

the support  $\{t, \alpha(t) = \alpha\}, f(\alpha)$ ;

$$\tau(q) = \min_{\alpha}(q\alpha - f(\alpha)); \quad (4)$$

see also [16]. In the literature,  $Z(a; q)$  is sometimes referred to as the partition function due to its analogy to the energy partition function in statistical mechanics. A monofractal refers to the case where  $\{\alpha\}$  is a singleton. The singularity spectrum is called multifractal when  $\{\alpha\}$  spans an interval.

## 2.2 WTMM-based JPFA of Fractal Correlation

In this section, the WTMM approach is generalized and applied in the JPFA of fractal correlation between multifractal singularity spectra. We present the application of JPFA of two data sets. The extension to more data sets is conceptually similar.

Consider  $x_1(t), x_2(t)$  and their respective sets of singularity exponent  $\{\alpha_1\}, \{\alpha_2\}$ . Let the maxima lines of  $|T_{\psi}[x_k]|$  at scale  $a$  be denoted as  $\mathcal{L}_k(a), k = 1, 2$ . A natural extension of the existing WTMM analysis is to consider a joint partition function of the form:

$$Z(a; q_1, q_2) = \sum_j C_{1,r(j)}^{q_1} C_{2,s(j)}^{q_2} \quad (5)$$

where  $C_{1,r}, C_{2,s}$  are the modulus maxima along the maxima lines  $l_{1,r} \in \mathcal{L}_1, l_{2,s} \in \mathcal{L}_2$ .

To realize (5), the maxima lines in  $\mathcal{L}_k, k = 1, 2$  must be paired up properly (so the index  $j$  can run). As in most correlation analyses, the goal is to characterize the property related to observing both singularity exponents  $\alpha_1$  and  $\alpha_2$ . In terms of the WTMM analysis, such information is contained in the modulus of the neighboring maxima lines. If the time coordinate of  $l_{k,j}(a)$  is denoted by  $t_{k,j}(a)$ , this means the coefficients  $C_{1,r}, C_{2,s}$  paired up in (5) can be determined by

$$|t_{1,r} - t_{2,s}| = \min_{r'}(|t_{1,r'} - t_{2,s}|) = \min_{s'}(|t_{1,r} - t_{2,s'}|) \quad (6)$$

Once (5) and (6) are established, similar procedure developed by Bacry et al. can be extended to characterize the geometry associated with the observation of  $\alpha_1$  and  $\alpha_2$ . In particular, based on  $C_{k,\lambda} \sim a^{\alpha_k(\lambda)}$ ,  $\lambda = r, s$  [15,17,18], (5) can be given by

$$Z(a; q_1, q_2) \sim \sum_j a^{q_1\alpha_1(r(j))+q_2\alpha_2(s(j))} = \int \int d\alpha_1 d\alpha_2 \mathcal{P}(\alpha_1, \alpha_2) a^{q_1\alpha_1+q_2\alpha_2} a^{-f(\alpha_1, \alpha_2)} \quad (7)$$

where  $\mathcal{P}(\alpha_1, \alpha_2)$  and  $f(\alpha_1, \alpha_2)$  are the probability density function and Hausdorff dimension of the support of  $(\alpha_1, \alpha_2)$ , respectively. Applying the standard argument of steepest descent in small  $a$ , one has

$$Z(a; q_1, q_2) \sim a^{\tau(q_1, q_2)} \quad (8)$$

where

$$\tau(q_1, q_2) = \min_{\alpha_1, \alpha_2} (q_1 \alpha_1 + q_2 \alpha_2 - f(\alpha_1, \alpha_2)). \quad (9)$$

Hence,  $\tau(q_1, q_2)$  and  $f(\alpha_1, \alpha_2)$  are Legendre transform pair:

$$\begin{aligned} \alpha_1 &= \partial \tau(q_1, q_2) / \partial q_1, \alpha_2 = \partial \tau(q_1, q_2) / \partial q_2, \\ f(\alpha_1, \alpha_2) &= \alpha_1(q_1, q_2)q_1 + \alpha_2(q_1, q_2)q_2 - \tau(q_1, q_2). \end{aligned} \quad (10)$$

where

$$q_1 = \partial f / \partial \alpha_1, q_2 = \partial f / \partial \alpha_2. \quad (11)$$

Finally, from (9)  $\sim$  (11), the correlation coefficient between  $\alpha_1, \alpha_2$  can be estimated using  $\tau(q_1, q_2)$ :

$$\rho = \frac{\text{cov}(\alpha_1, \alpha_2)}{\sigma_{\alpha_1} \sigma_{\alpha_2}} = - \frac{\frac{\partial^2 \tau}{\partial q_1 \partial q_2}}{\sqrt{\left[ \frac{\partial^2 \tau}{\partial q_1^2} \frac{\partial^2 \tau}{\partial q_2^2} \right]}} \Bigg|_{q_1=q_2=0} \quad (12)$$

where cov denotes the covariance and  $\sigma_\lambda$  denotes the standard deviation of  $\lambda$ . This expression will be used in the next section to compare with the numerical result.

In practice, the Legendre transform (10) relies on using  $\tau$  estimated from (8). However, there are known factors, such as lacunarity [19, 20], that introduce oscillatory, scale dependent, prefactor. This results in the poor estimate of  $\tau(q_1, q_2)$ . A remedy to this problem can be motivated by an alternative approach equivalent to the canonical ensemble in statistical mechanics [20]. Let

$$\nu(j, a; q_1, q_2) = \frac{C_{1,r(j)}^{q_1} C_{2,s(j)}^{q_2}}{Z(a; q_1, q_2)}. \quad (13)$$

Then, it can be shown (Appendix):

$$\mathbf{A}_1(a; q_1, q_2) = \sum_j \nu(j, a; q_1, q_2) \log(C_{1,r(j)}) \sim a^{\alpha_1(q_1, q_2)} \quad (14)$$

$$\mathbf{A}_2(a; q_1, q_2) = \sum_j \nu(j, a; q_1, q_2) \log(C_{2,s(j)}) \sim a^{\alpha_2(q_1, q_2)} \quad (15)$$

$$\mathbf{F}(a; q_1, q_2) = \sum_j \nu(j, a; q_1, q_2) \log(\nu(j, a; q_1, q_2)) \sim a^{f(\alpha_1, \alpha_2)}. \quad (16)$$

## 2.3 JPFA and Relative Multifractal Analysis

Relative multifractal analysis and similar ideas were developed to characterize fractal correlation between fractal measures. The main idea is to replace the use of Lebesgue measure in the traditional fractal analysis [5,6,7,8]. Specifically, consider the partition functions of multifractal measures  $\pi$  and  $\mu$

$$\sum_{A \in \mathcal{H}} \pi(A)^q \sim |A|^{\tau_\pi(q)}, \quad \sum_{A' \in \mathcal{H}'} \mu(A')^q \sim |A'|^{\tau_\mu(q)} \quad (17)$$

where  $\mathcal{H}, \mathcal{H}'$  denote generic partitions of the support and  $|\cdot|$  denote the Lebesgue measure of the set. To examine the extent to which the singularity of  $\pi$  correlate with  $\mu$ , the sets which scale as a power law will now be characterized by using  $\pi$ . For example, the partition function of  $\pi$  is now written as

$$\sum \pi(A)^q \mu(A)^{-\mathbf{t}(q)} \sim O(|A|) \quad (18)$$

where the “big  $O$ ” describes the order relationship  $O(|A|) \rightarrow \text{const.}$  as  $|A| \rightarrow 0$ . Define  $\tau_{\pi/\mu}(q) = \sup\{\mathbf{t}(q)\}$  for which (18) holds. The relative multifractal spectrum is obtained via the Legendre transform of  $\tau_{\pi/\mu}$ . It characterizes the support of the singular behaviour of the form  $\pi \sim \mu^{\alpha_{\pi/\mu}(q)}$  where  $\alpha_{\pi/\mu}(q) = d\tau_{\pi/\mu}(q)/dq$ . The relative multifractal analysis can draw a much sharper distinction between  $\pi$  and  $\mu$ . For example,  $\tau_{\pi/\mu}(q)$  is nonlinear when  $\pi \neq \mu$  and  $\tau_{\pi/\mu}(q) = q - 1$  when  $\pi = \mu$ ; see [6] for more details.

Comparison of (18) with (5) and (8) suggests  $\tau_{\pi/\mu}$  can be obtained as the level set of  $\tau(q_1, q_2) = 0$  where

$$q_2 = -\tau_{\pi/\mu}(q_1). \quad (19)$$

To assure finite generalized dimension,  $\tau_{\pi/\mu}(1) = 0$  and, thus, the level set  $\tau(q_1, q_2) = 0$  must pass through  $(q_1, q_2) = (1, 0)$ . This property can also be directly seen for the multinomial processes (next section).

Similarly, by switching the role of  $q_1, q_2$ , the singular behaviour of  $\mu$  “viewed” by  $\pi$  can be described. With the same argument, this is characterized by  $\tau_{\mu/\pi}(q_2)$  defined from the same level set  $\tau(q_1, q_2) = 0$  where  $q_1 = -\tau_{\mu/\pi}(q_2)$ . It may be useful to point out that  $\tau_{\pi/\mu}, \tau_{\mu/\pi}$  on the  $q_1 \times q_2$  plane are nothing but mirror images of the contour of  $\tau(q_1, q_2) = 0$  about  $q_2 = 0$  and  $q_1 = 0$  axes, respectively. In general,  $\tau_{\pi/\mu}(q) \neq \tau_{\mu/\pi}(q)$ , although they are derived from the same level set.

### 3 Numerical Experiments

To test if the WTMM-based JPFA can reliably characterize fractal correlation, numerical experiments are conducted on the coupled random binomial cascades studied by Meneveau et al. [1].

The first cascade, denoted as  $\pi$ , is generated by weights  $p_0, p_1$  (referred to as  $\pi$ -cascade). Let  $I_{r_1, \dots, r_J}$  denote an interval segment generated in the  $J$ th iteration where  $r_i \in \{0, 1\}$  and  $\sum r_i 2^{-i}$  is the based-2 coarse-grained representation of any  $x \in I_{r_1, \dots, r_J}$ . By the multiplicative rule,  $\pi(I_{r_1, \dots, r_J}) = \prod_{j=1}^J p_{r_j}$ . The second cascade, denoted as  $\mu$ , is generated by weights  $m_0, m_1$  (referred to as the  $\mu$ -cascade). With the same addressing scheme, one has  $\mu(I_{s_1, \dots, s_J}) = \prod_{j=1}^J m_{s_j}$  where  $s_i \in \{0, 1\}$ .

In the numerical experiment, a parameter  $g$  and a uniform random variable  $\gamma$  in  $[0, 1]$  are used to control the degree of coupling or correlation between the cascades. Let  $I_L, I_R$  be the new segments created from their parent segment of the previous generation. If  $\gamma < g$ , the weights assigned to  $I_L, I_R$  of the  $\mu$ -cascade will depend on exactly how the weights of the  $\pi$ -cascade are assigned. The rule for this dependence is that  $p_0$  and  $m_0$  ( $p_1$  and  $m_1$ ) are always assigned at the same time. For example, if  $p_0$  is assigned to  $I_L$  ( $I_R$ ) of the  $\pi$ -cascade,  $m_0$  will be assigned to  $I_L$  ( $I_R$ ) of the  $\mu$ -cascade and similarly for  $p_1$  and  $m_1$ . If  $\gamma \geq g$ , the weight assignment for the cascades will be completely independent from each other. This way, the fractal generating mechanisms of the cascades are completely dependent of each other when  $g = 1^+$  and independent of each other when  $g = 0^-$ .

The coarse-grained joint partition function for the coupled cascades can be defined based on (5):

$$Z_J(a; q_1, q_2) = \sum \pi(I_{r_1, \dots, r_J})^{q_1} \mu(I_{r_1, \dots, r_J})^{q_2}.$$

From the combination of  $\gamma$  completely dependent and  $(1 - \gamma)$  independent proportions,  $Z_J$  is derived explicitly as

$$Z_J(a; q_1, q_2) \sim (2Y)^J \tag{20}$$

where

$$Y = \gamma \left( \frac{p_0^{q_1} m_0^{q_2} + p_1^{q_1} m_1^{q_2}}{2} \right) + (1 - \gamma) \left( \frac{p_0^{q_1} m_0^{q_2} + p_1^{q_1} m_0^{q_2} + p_0^{q_1} m_1^{q_2} + p_1^{q_1} m_1^{q_2}}{4} \right). \tag{21}$$

As  $J \rightarrow \infty$ ,  $Z_J \rightarrow Z$  and the analytical  $\tau(q_1, q_2)$  can be obtained from (21) as

$$\tau(q_1, q_2) = -\log_2(2Y) \tag{22}$$

By (10), the analytical  $\alpha_1, \alpha_2$  and  $f(\alpha_1, \alpha_2)$  can be found [21]. These results will be compared to the numerical ones below.

In the numerical experiments,  $p_0 = 0.2, p_1 = 0.8$  and  $m_0 = 0.4, m_1 = 0.6$  are used to generate the  $\pi$ - and  $\mu$ -cascades for  $g = 1, 0.8, 0.3, 0$ . For each  $g$  value, 30 pairs of  $\pi, \mu$  cascades, each of 16,384 points are generated. The first derivative of the Gaussian wavelet has been used as the analyzing wavelet in this work. Using higher order derivative of the Gaussian wavelet does not create qualitatively different result. In practice, the modulus maxima and the maxima lines of the individual cascade are first obtained. The modulus maxima from the nearest maxima lines are then paired up according to (6) and used in (5) to define the joint partition function. The numerical  $\alpha_1, \alpha_2$  and  $f(\alpha_1, \alpha_2)$  are finally estimated following (13)  $\sim$  (16) and  $\tau(q_1, q_2)$  is determined following (9).

Typical maxima lines of the coupled cascades are shown in Fig. 2. It is observed that the maxima lines are “aligned” when the fractal generation is completely dependent at  $g = 1$  and begin to “mis-align” for  $g < 1$ . The power law scaling of  $Z(a; q_1, q_2)$  are found in all cases (Fig. 3). In Fig. 4, contours of the level set of  $f(\alpha_1, \alpha_2)$  are shown on the  $\alpha_1 \times \alpha_2$  plane. It is evident that the geometry of the contour lines vary systematically with the  $g$  value. When the fractal generating mechanisms are completely dependent of each other ( $g = 1$ ),  $f(\alpha_1, \alpha_2)$  describes a one-dimensional curve supported by the functional relationship  $\alpha_1(\alpha_2)$ . This is expected as any spiking pattern in one cascade automatically implies the same for the other. As a result, the maxima lines will converge at the same location in the time-scale plane. This establishes the one-to-one relationship of observing the exponents  $\alpha_1$  and  $\alpha_2$ . In general ( $g < 1$ ),  $f(\alpha_1, \alpha_2)$  describes a two-dimensional surface, which gives rise to oval-shape contours (Figs. 4b, 4c, 4d). This means that the observation of  $\alpha_1$  can take place simultaneously for a range of  $\alpha_2$ . As a result, the contour “opens up” and becomes the largest when the fractal generations are completely independent from each other ( $g = 0$ ). For  $g = 0$ , there is a perfect alignment of the axes of the contour and the  $\alpha_1 = 0$  and  $\alpha_2 = 0$  axes (Fig. 4d). Superimposed on these figures are the analytical  $f(\alpha_1, \alpha_2)$  derived by the Legendre transform of (22). It is seen that the WTMM-based JPFA agrees well with the theory. To further the check of the WTMM-based approach, the correlation of  $\alpha_1, \alpha_2$  is estimated using the numerical  $\tau(q_1, q_2)$ . This is to compare with the analytical  $\rho = g$  obtained by substituting (22) into (13). The result is summarized in Table 1. Again, good agreement is found.

$g$	0.0	0.3	0.8	1.0
$\rho$	0.016	0.280	0.775	0.838

TABLE 1 Numerical  $\rho$  value for  $g = 0, 0.3, 0.8, 1.0$  (Note, in theory,  $\rho = g$ ).

To test the robustness of the algorithm, different analyzing wavelets are also used to study the coupled cascades. While deviations are expected to result from the choice of the analyzing wavelets, no qualitatively different result is found. Fig. 5 demonstrates the coupled cascades of  $g = 0.8$ . It is evident that the contour lines of  $f(\alpha_1, \alpha_2)$  estimated from different analyzing wavelets are all fallen onto the theoretical contour lines.

Finally, from the numerical data,  $\tau_{\pi/\mu}(q_1)$  is estimated from the level set  $\tau(q_1, q_2) = 0$ . We then conduct the relative multifractal analysis using the deterministic algorithm proposed by Riedi and Scheuring [6]. In Fig. 6, the  $\tau_{\pi/\mu}(q_1)$  estimated by these two different approaches are shown to match well. The agreement confirms that the relative multifractal spectrum is contained in the level sets of  $\tau(q_1, q_2)$ . Similar match is also found for  $\tau_{\mu/\pi}$  (not shown).

## 4 Concluding Remarks

In applications, the ability to characterize fractal correlation in the data fluctuation could provide insights into the underlying complex dynamics.

In this work, a WTMM-based technique is introduced for the first time to estimate the fractal correlation in the framework of joint partition function analysis proposed by Meneveau et al. [1]. As WTMM has been proven an effective tool to extract the singularity spectrum of certain important class of fractal functions [15, 16], it is shown that the extension developed in this work also capture accurately the fractal correlation of data fluctuation. We also found another leading idea developed for the fractal correlation analysis, relative multifractal spectrum, can be considered as a special case of JPFA at a particular parameter setting.

**Acknowledgment** This research is supported by Natural Science and Engineering Research Council of Canada.

## APPENDIX

First, consider (14). By (8) and (10), one has

$$\partial Z(a; q_1, q_2)/\partial q_1 \sim a^{\tau(q_1, q_2)} \log(a) \partial \tau(q_1, q_2)/\partial q_1 = a^{\tau(q_1, q_2)} \log(a) \alpha_1. \quad (A.1)$$

Note the prefactor  $\log(a)\alpha_1$  in (A.1) that varies logarithmically with  $a$ . From (A.1), one has

$$\sum_j \nu \log(|C_{1,j}|) = \frac{\partial Z/\partial q_1}{Z}. \quad (A.2)$$

Equation (14) follows after substituting (A.1) into (A.2). Note also the prefactor in (8) is canceled out in (A.2). The derivation for (15) is the same.

Based on (A.2), one has

$$\sum \nu \log(\nu) = q_1 \frac{\partial Z/\partial q_1}{Z} + q_2 \frac{\partial Z/\partial q_2}{Z} - \log(Z). \quad (A.3)$$

Again, using (A.1), (16) results after substituting (10) into the above.

## Reference

- [1] C. Meneveau et al., *Phys. Rev. A* **41**, 894 (1990).
- [2] J.O. Fortrat et al., *Auton. Neurosci.* **86**, 192 (2001); also general review in Task Force of the ESC and NASPE, *Euro. Heart J.* **17**, 354 (1996).
- [3] J. Lévy-Léhel and R. Riedi, Fractal in Engineering, Eds. J. Lévy-Léhel, E. Lutton, C. Tricot, *Springer Verlag*, London, 185 (1997).
- [4] Y. Pesin, Dimension theory in dynamical systems: contemporary views and applications, Chicago Lectures in Mathematics, *Chicago Univ. Press* (1997).
- [5] J. Lévy-Léhel and R. Vojak, *Adv. Appl. Math.* **20**, 1 (1998).
- [6] R.H. Riedi and I. Scheuring, *Fractals* **5**, 153 (1997).
- [7] G. Brown et al., *J. Stat. Phys* **66**, 775 (1992).
- [8] J. Cole, *Chaos, Solitons & Fractals* **11**, 2233 (2000).
- [9] H.G.E. Hentschel and I. Procaccia, *Physica D* **8**, 435 (1983).
- [10] M.H. Halsey et al., *Phys. Rev. A* **33**, 1141 (1986).
- [11] D. Schertzer and S. Lovejoy, Space/Time Variability and Interdependencies in Hydrological Processes, Ed. R.A. Feddes, *Cambridge Univ. Press*, 153 (1995).
- [12] A.N. Kravchenko et al., *Agron. J.* **92**, 1279 (2000).
- [13] T.B. Zeleke et al., *Soil Sci. Soc. Am. J.* **69**, 1691 (2005).

- [14] W-X. Zhou and D. Sornette, arXiv:cond-mat/0408600 (2004).
- [15] E. Bacry et al., *J. Stat. Phys* **70**, 635 (1993).
- [16] S. Jaffard, *SIAM J. Math. Anal.* **28**, 944 (1997).
- [17] S. Mallat and W.L. Hwang, *IEEE Trans. Info. Theory* **38**, 617 (1992).
- [18] J.F. Muzy et al. *Phys. Rev. E* **47**, 875 (1993).
- [19] C. Meneveau and K.R. Sreenivasan, *Phys. Lett. A* **137**, 103 (1989).
- [20] A. Chhabra and R.V. Jensen, *Phys. Rev. Lett.* **62**, 1327 (1989).
- [21] A. Sharif, *Master Thesis*, Department of Mech. & Ind. Eng., Ryerson University (2006).

## Figure Captions

Fig. 1. Multifractal analyses of 3-adic  $\pi$ -cascade of weights 0.2, 0.28, 0.52 (symbol "o") and 5-adic  $\mu$ -cascade of weights 0.09463, 0.1200, 0.1800, 0.2217, 0.3837 (symbol "+"). (a)  $\tau_\pi(q)$  and  $\tau_\mu(q)$ ; (b)  $f_\pi(\alpha)$  and  $f_\mu(\alpha)$ .

Fig. 2. Typical maxima lines in the time-scale plane from one of the 30 sets of  $\pi$ - ("o") and  $\mu$ -cascades ("+") with coupling parameter  $g = 1.0, 0.8, 0.3, 0.0$  (top to bottom). Notice the perfect alignment of maxima lines for the completely dependent cascades ( $g = 1$ ). First derivative of the Gaussian wavelet is used in the numerical calculation.

Fig. 3  $\log(\mathbf{A}_1)$ ,  $\log(\mathbf{A}_1)$  and  $\log(\mathbf{F})$  vs.  $\log(a)$  plots of a typical case of the coupled cascades with  $g = 0.8$ . The straight lines describes the power laws at  $(q_1, q_2) = (3, -2), (4, 0), (0, 0), (-1, 3)$  (top to bottom). Regression lines are shown as solid lines. The slope of the regression lines are estimated as  $\alpha_1, \alpha_2$  and  $f(\alpha_1, \alpha_2)$  based on (14)–(16).

Fig. 4 Averaged contour lines of numerical  $f(\alpha_1, \alpha_2) = C$  for  $C = 0.6$  (outer contour), 0.75, 0.9 (inner contour). Theoretical contour lines are shown as solid lines. The averaging over 30 pairs of  $\pi$  and  $\mu$  cascades is shown as "o" ( $C = 0.6$ ), "•" ( $C = 0.75$ ) and " $\Delta$ " ( $C = 0.9$ ). Error bars of one standard deviation from selected data points are shown. They are obtained from the ensemble of contour line points in a uniform grid on the  $q \times p$ . The corresponding  $g$  values are (a) 1, (b) 0.8, (c) 0.3, (d) 0.

Fig. 5 Averaged contour lines of numerical  $f(\alpha_1, \alpha_2) = C$  for  $g = 0.8$  and  $C = 0.6$  (outer contour), 0.75, 0.9 (inner contour). The analyzing wavelets are ... ("o"), ... ("+"), ... (" $\Delta$ "). Theoretical contour lines are shown as solid lines. Error bars of one standard deviation from selected data points are shown. Compare with Fig. 4b.

Fig. 6  $\tau_{\pi/\mu}(q)$  estimated by WTMM-based JPFA ('o') method (from the contour line of  $\tau(q, p) = 0$ ) and the deterministic algorithm proposed (solid line); see text. The solid lines shown are based on the ensemble average with  $\pm 3$  standard deviation boundaries plotted as long-dashed lines. The  $g$  values are (a) 1, (b) 0.8, (c) 0.3, (d) 0.

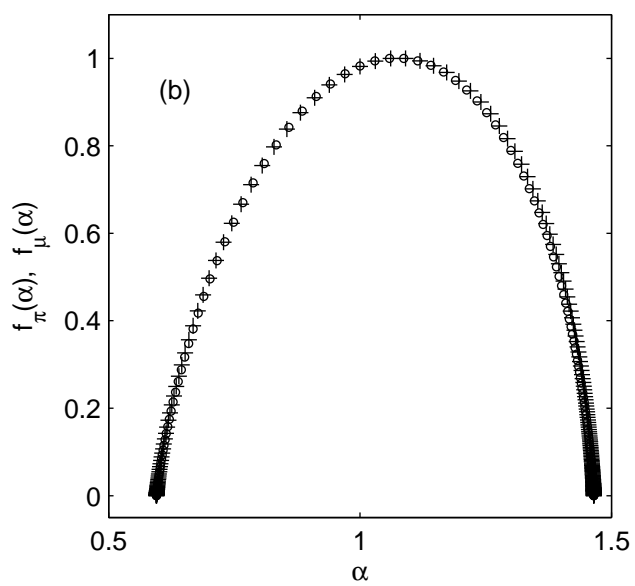
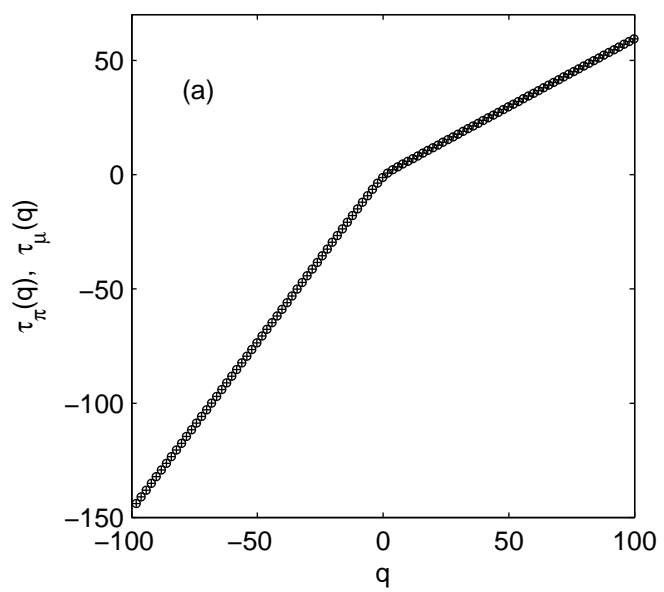


Fig. 1

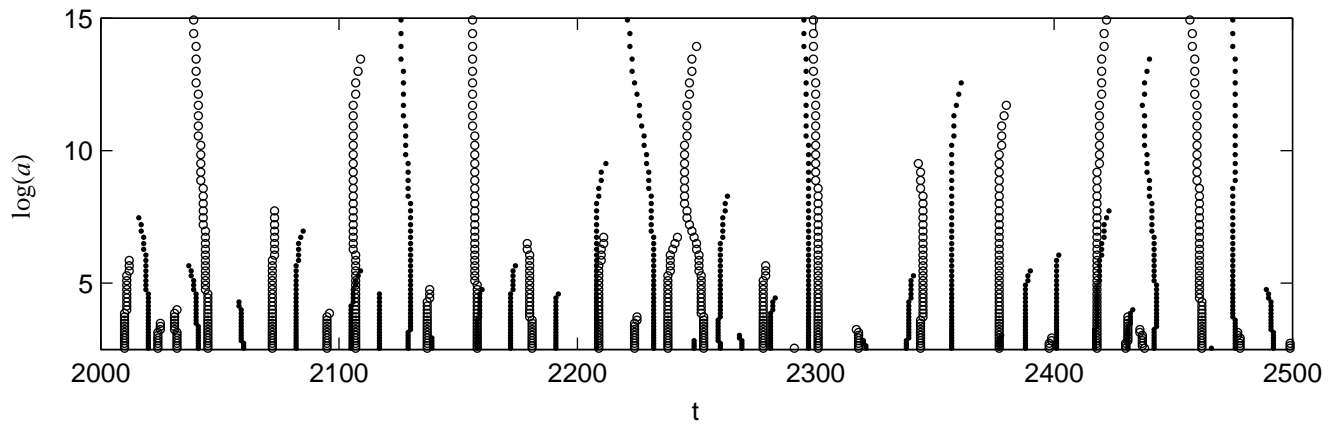
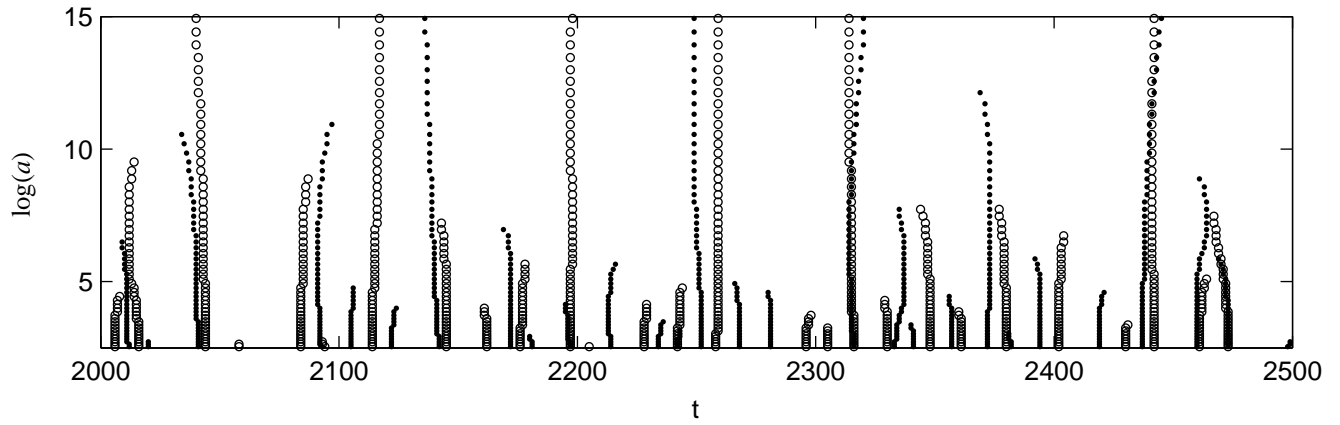
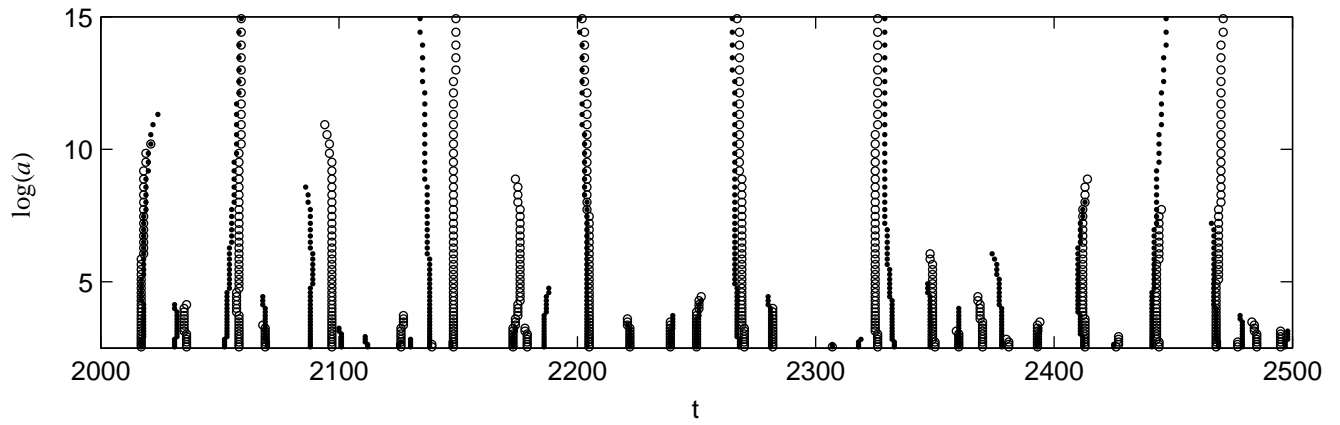
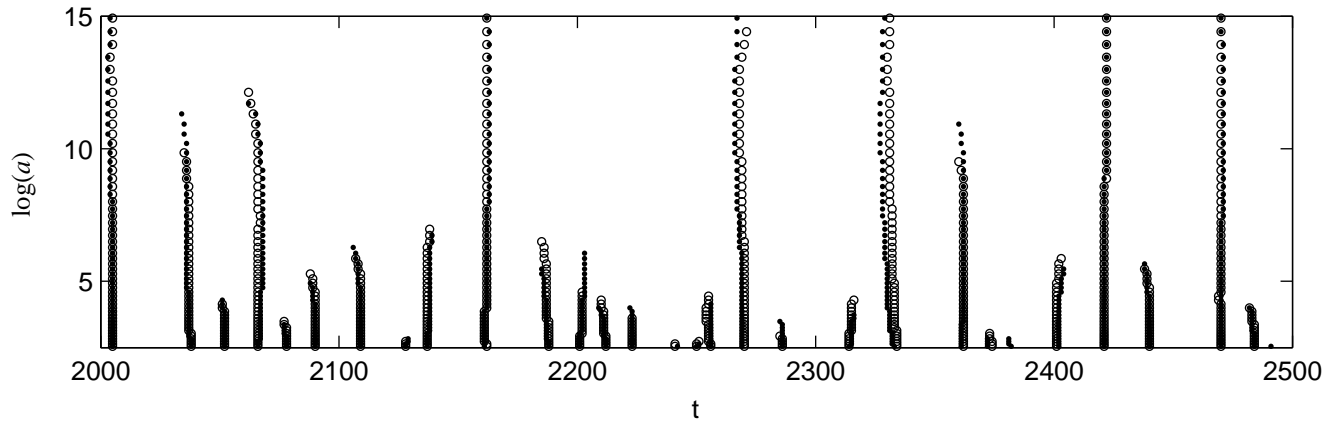


Fig. 2

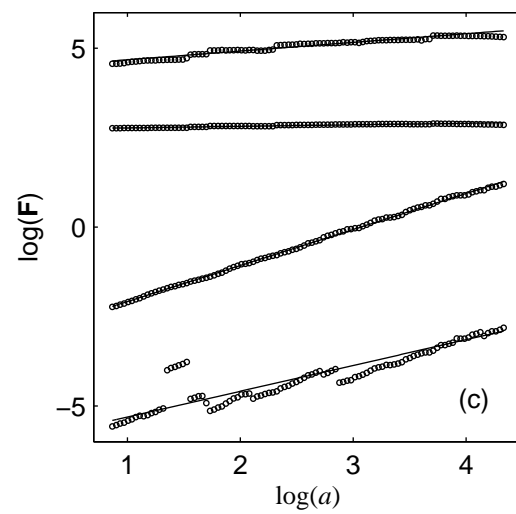
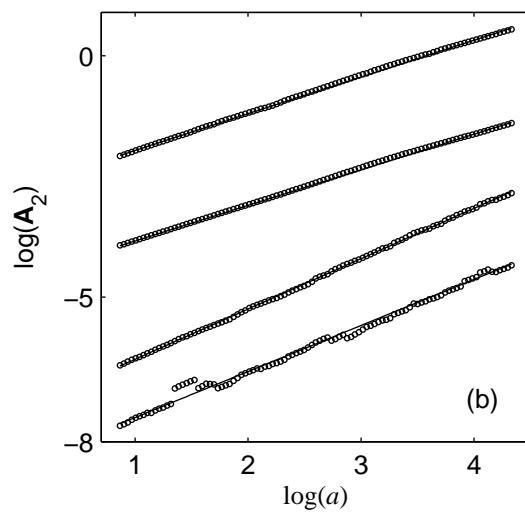
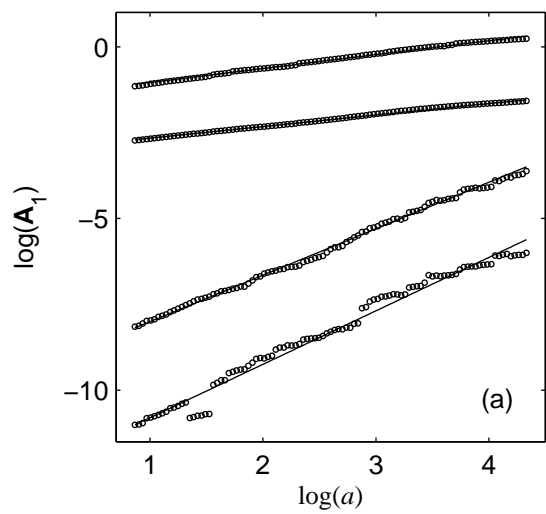


Fig. 3

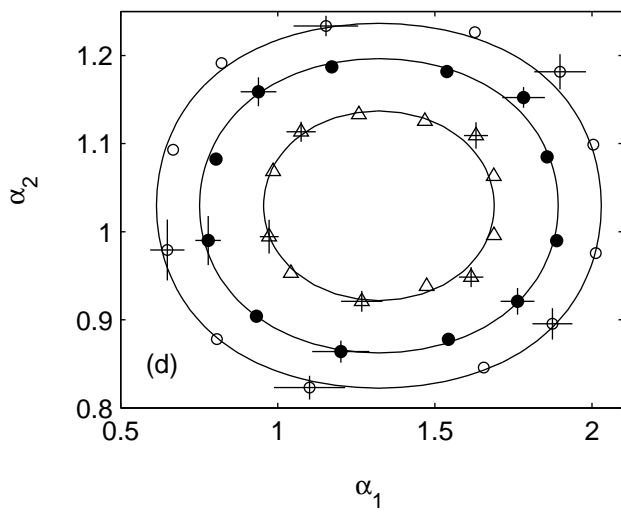
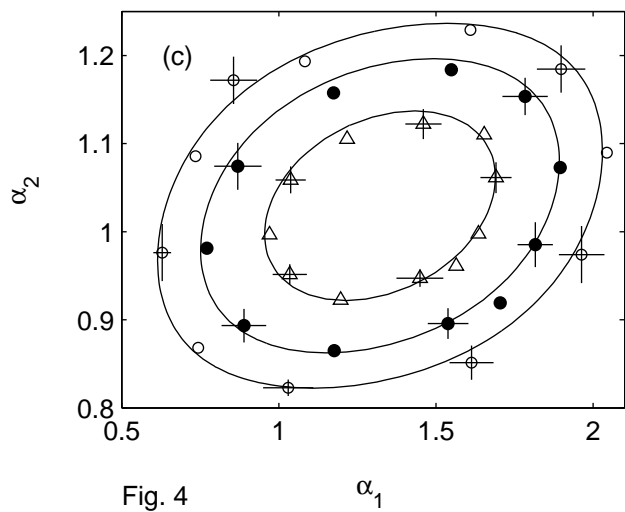
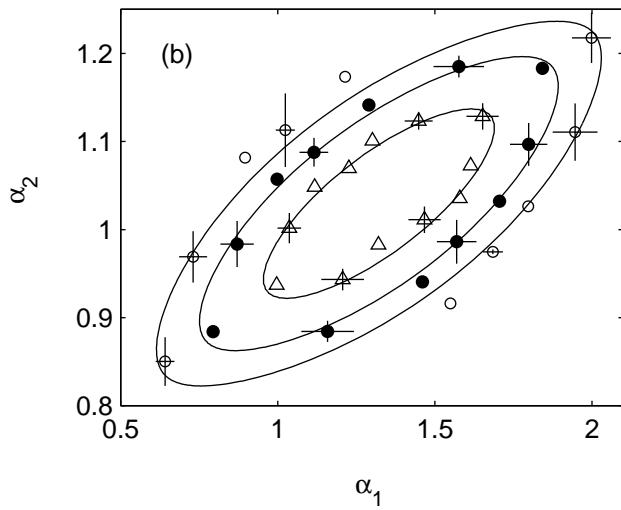
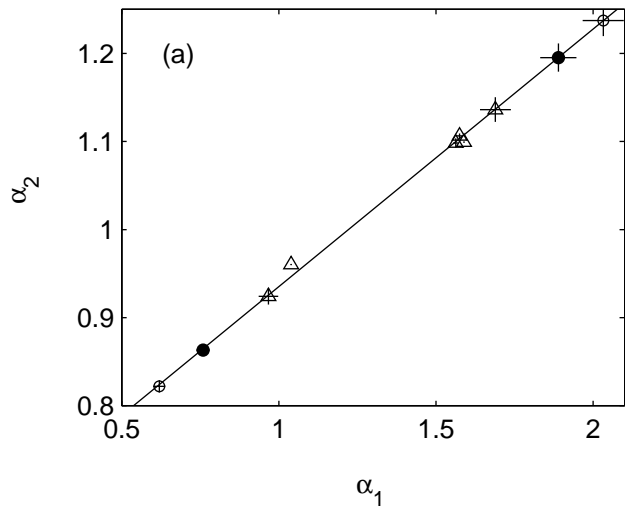


Fig. 4

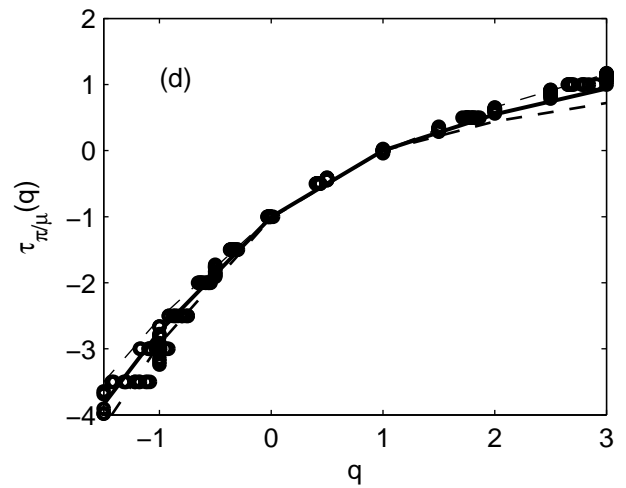
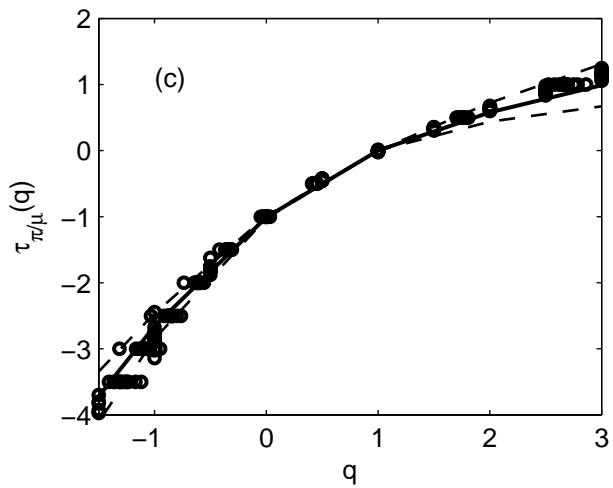
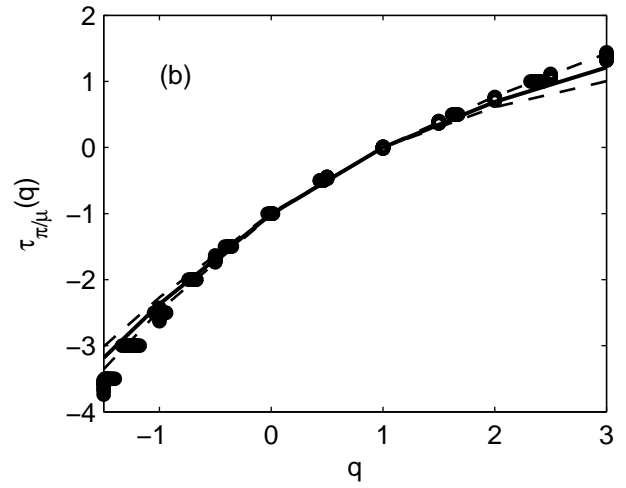
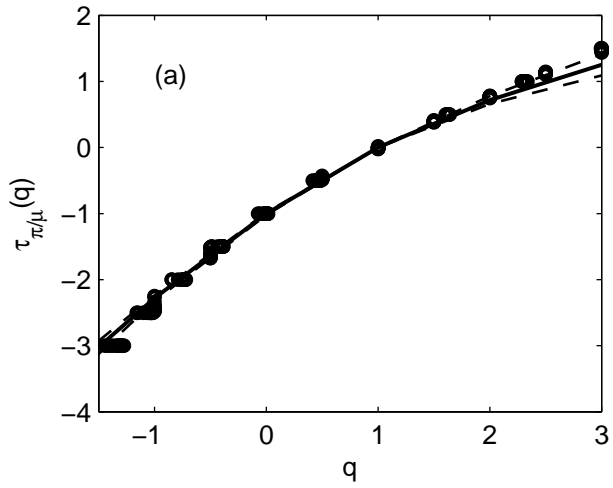


Fig. 5